Numerical study of fast-ion loss in the Experimental Advanced Superconducting Tokamak

Yongxin Zhu(朱永昕)[1,2], Wei Zhang(张伟)[1,†], Kunihiro Ogawa(小川国大)[3,4], Mitsutaka Isobe(磯部光孝)[3,4,5], Yifeng Zheng(郑艺峰)[1], Zhengshuyan Wang(王郑树彦)[1], Huapeng Zhang(张华朋)[6], Xinjun Zhang(张新军)[1], Lunan Liu(刘鲁南)[1], Yaoyao Guo(郭垚垚)[1], Lin Ai(艾琳)[1], Sichun Qiu(邱思淳)[1], Tao Jin(金韬)[1], Yuhao Jiang(蒋宇昊)[1], Liuxin Li(李柳欣)[1], Yujia Deng(邓羽佳)[1], and Zian Zhang(张梓安)[1]

[1] *Institute of Plasma Physics, Hefei Institutes of Physical Science, Chinese Academy of Sciences, Hefei* 230031, *China*
[2] *University of Science and Technology of China, Hefei* 230026, *China*
[3] *National Institute for Fusion Science, National Institutes of Natural Sciences, Toki* 509-5292, *Japan*
[4] *The Graduate University for Advanced Studies, SOKENDAI, Toki* 509-5292, *Japan*
[5] *Mahasarakham University, Maha Sarakham* 44150, *Thailand*
[6] *Department of Plasma Physics and Fusion Engineering, School of Nuclear Science and Technology, University of Science and Technology of China, Hefei* 230026, *China*

(Received 13 November 2025; revised manuscript received 25 December 2025; accepted manuscript online 4 January 2026)

The plasma transport analysis code TRANSP and full-orbit following code LORBIT were used to study fast-ion loss in the Experimental Advanced Superconducting Tokamak (EAST) under varying discharge parameters and heating scenarios, considering the synergistic effect of neutral beam injection (NBI) and ion cyclotron range of frequency (ICRF). To more faithfully simulate fastion loss processes, the axisymmetric twodimensional poloidal contours of the EAST first wall and the antenna limiters were used as the loss boundary and then stretched toroidally to construct a threedimensional boundary structure. Results indicate that the fast ion loss diminishes as the plasma current ($I_{\rm P}$) and toroidal magnetic field ($B_{\rm t}$) increase. Furthermore, the impact of different magnetic configurations on the fast-ion loss was considered. Increasing the distance between the antenna and the separatrix ($R_{\rm gapout}$) can significantly reduce the fast-ion loss. When the toroidal magnetic field was reversed, i.e., $B_{\rm t} > 0$, the lower single-null configuration was more effective in mitigating the fast-ion loss than double-null and upper single-null configurations. A significant reduction in the fraction of fast-ion loss was observed when an outer strike point was positioned on the vertical target plate. Finally, the effects of varying NBI energies, injection angles, and ICRF antenna phases were investigated. The results indicate that, within certain limits, fast-ion loss decreases as the NBI injection angle increases, whereas higher NBI injection energies lead to more fast ion escape. In contrast, variations in the ICRF antenna phase exert only a marginal effect on fast-ion loss.

Keywords: fast ion, orbit, tokamak

PACS: 52.20.Dq, 52.50.Gj, 52.55.Fa, 52.65.Cc

DOI: 10.1088/1674-1056/ae3307 **CSTR:** 32038.14.CPB.ae3307

1. Introduction

Fast ions generated by auxiliary heating, such as neutral beam injection (NBI) and ion cyclotron range of frequency (ICRF), play crucial roles in enhancing current drive and plasma heating efficiency in magnetically confined fusion devices. Neutral atoms injected into plasma via NBI are converted into fast ions via charge exchange or ionization.[1,2] Additionally, the electric field from the ICRF effectively accelerates the fast ions near higher-order harmonic resonance layers.[3] These fast ions are captured by the magnetic field and transfer energy to electrons and ions in the background plasma via Coulomb collisions,[4] thereby contributing to plasma heating. To achieve the self-sustained combustion of magnetically confined plasma, fast ions must be confined within a magnetic field region for a sufficient duration to fully interact with and heat the main plasma, and drive the current. However, fast ion loss can occur in fusion reactors due to magnetohydrodynamic (MHD) instabilities,[5,6] toroidal field ripple,[7,8] first orbits[9] and collisions.[10] A significant loss of fast ions not only greatly reduces the plasma heating efficiency but also causes severe thermal damage to the first wall of the vacuum vessel, potentially leading to discharge termination.[11,12] Therefore, the confinement and loss of fast ions is one of the important topics in fusion research.

The Experimental Advanced Superconducting Tokamak (EAST) is currently equipped with two NBI systems (NBI1 and NBI2), each consisting of left and right beamlines.[13] Each beamline is equipped with a positive ion source capable of delivering 2 MW of power to the plasma, with a beamline energy ranging from 50 keV to 80 keV.[14] Additionally, EAST is equipped with a 25–70 MHz ICRF auxiliary heating system, which features eight independent power lines, each capable of delivering 1.5 MW of RF power to the plasma. Apart from

†Corresponding author. E-mail: zw@ipp.ac.cn

© 2026 Chinese Physical Society and IOP Publishing Ltd. All rights, including for text and data mining, AI training, and similar technologies, are reserved.

CPB Online in Press

the two auxiliary heating methods described above, EAST is equipped with electron cyclotron resonance heating (ECRH) and low hybrid (LH) heating systems. The locations of the NBI, ICRF, LH, and ECRH systems are shown in Fig. 1. The injection angles of NBI1 and NBI2 are 19.5° and 17°, respectively. To study fast-ion loss in the EAST, several types of fast ion loss detectors (FILDs) were deployed to measure NBI fast ion loss under both co- and counter-rotation conditions.[15] Additionally, infrared cameras and neutron diagnostics installed on the EAST can also be used to investigate fast-ion loss and transport. Alongside experimental studies, numerous numerical simulations have also aimed to self-consistently calculate rapid ion loss in the presence of ICRF and NBI. Many orbit-following codes, such as LORBIT,[16] PTC,[17,18] ISSDE,[19,20] ASCOT,[21] SPIRAL[22] and TGCO[23] have been developed to study the loss and transport of fast ions. These orbit tracking codes differ in both their underlying physical models and principal application domains. PTC and ASCOT are general-purpose Monte Carlo platforms designed for simulating fast ions. PTC performs full-orbit and guiding-center calculations of high-energy particles (e.g., alpha particles, NBI ions, and runaway electrons) in tokamaks, and is particularly suited to evaluating confinement and transport in three-dimensional magnetic configurations subject to MHD perturbations. ASCOT, in contrast, flexibly switches between guiding-center and full-orbit descriptions. It integrates detailed models for Coulomb collisions, three-dimensional ripple fields, complex first-wall geometry, and external sources such as NBI and ICRF heating, thereby providing a comprehensive framework for investigating minority-species kinetics and transport. LORBIT, by comparison, is optimized for high-resolution Lorentz-force orbit integration and particle-loss assessment from specified initial distributions within realistic three-dimensional magnetic and wall geometries. It is commonly employed as a post-processing module for integrated transport codes such as TRANSP, emphasizing the detailed characterization of device-specific orbit topologies and losses, while using simplified collision treatments and typically accounting for RF effects indirectly through external coupling. TCGO specializes in simulating NBI fast-ion deposition, thermalization, and initial spatial distributions, and excels in analyzing deposition power profiles and the characteristics of initial orbits.

In a previous study on the EAST, Wu *et al.* performed numerical simulations of deuterium beam ions, demonstrating that counter-current beam injection results in a significantly larger prompt loss fraction than co-injection.[24] Song *et al.* numerically investigated the loss of ions implanted by a neutral beam heated with ICRF.[25,26] The results showed that the ICRF waves altered the orbital distributions of the beam ions, causing an increase in trapped ions and fast ion loss. Xu *et al.* conducted numerical simulations of fast-ion loss in the presence of resonant magnetic perturbations (RMPs) and toroidal field ripples. They found that the fast-ion loss increases almost linearly with the coil current of the RMPs, and that collisions can enhance the loss of fast ions owing to the synergistic effect of RMPs and pitch scattering.[17] In the presence of RMPs, the loss zone of the NBI fast ions was primarily concentrated on low field sides near edges.[27] Zheng *et al.* studied the slow down and loss of fast ions resulting from Coulomb collisions.[20] However, research on fast-ion loss under varying magnetic field parameters and different NBI heating conditions in the EAST is limited. To provide a reference for plasma physics experiments on the EAST, we used the TRANSP[28,29] and LORBIT codes to calculate fast-ion loss under different conditions with NBI + ICRF synergy. The distributions of the ICRF-heated NBI ions were obtained via integrated calculations using the NUBEAM[30,31] and TORIC[32,33] modules of the TRANSP code. In particular, fast ions were considered lost when they collided with the first wall or limiter, rather than when they are outside the last closed flux surface (LCFS).

The remainder of this paper is outlined as follows. Descriptions of the code and calculation scheme are presented in Section 2. Numerical results of fast-ion loss in EAST are presented and discussed in Section 3. Main results are summarized in Section 4.

2. Setups for calculation

The boundary conditions employed in most fast-ion loss simulations in EAST typically assume an annular, uniform first wall boundary. However, in reality, the first wall at the mid-plane often consists of limiters designed to protect antennas and windows from potential damage. In this study, we have, for the first time on EAST using LORBIT, incorporated the realistic three-dimensional first-wall structure and limiter geometry into the boundary conditions for fast-ion loss simulations under NBI and ICRF synergistic heating scenarios. The limiters are located at ports B and E, four limiters at ports I and N, and a main limiter between ports G and H, as shown in Fig. 1. As shown in Fig. 2, the IC limiters at ports I and N are positioned radially at the same location, whereas the LH limiter at port B was 4.5 cm further from the plasma than the limiter at port E, meaning that the limiter at port E was closer to the plasma. The main limiter was the closest to the major plasma, followed by the IC limiters and the LH limiters at port; the LH limiter at port B was farthest from the major plasma. The limiters were modeled as axisymmetric two-dimensional poloidal contours that were stretched along the toroidal direction, based on their nominal positions and cross-sectional shapes. Although this approximation does not resolve toroidally localized features, it preserves the essential

CPB Online In-Press

radial and poloidal extents of each limiter, enabling a computationally efficient yet physically meaningful assessment of fast-ion loss patterns.

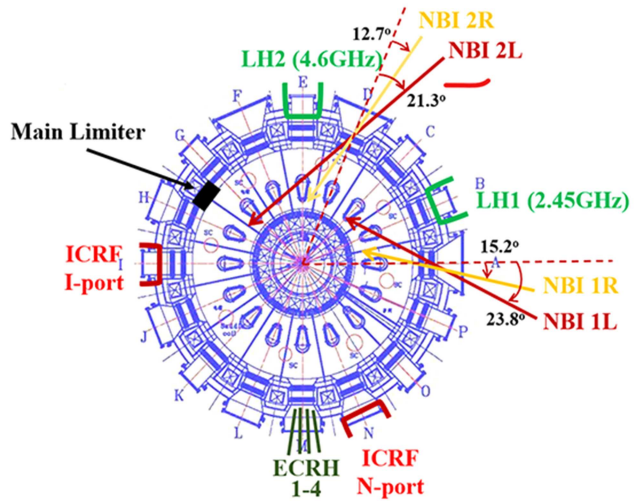


Fig. 1. Top view of the EAST tokamak, including the configurations of ICRF, NBI, ECRF, LH heating. NBI1 and NBI2 are located on ports A and D, respectively, and both are co-current. LH1 and LH2 with frequencies of 2.45 GHz and 4.6 GHz, respectively, are located on ports B and E, respectively. Two ICRF antennas are positioned at ports I and N, and the ECRF is located at port M.

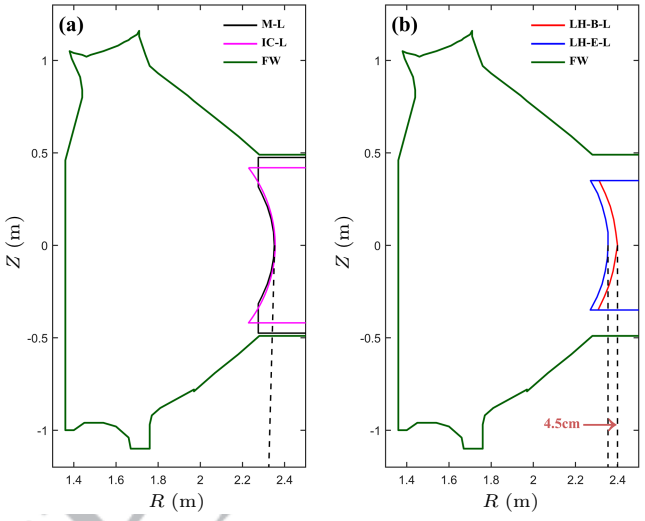


Fig. 2. Distribution of limiter positions on the poloidal view: (a) ion cyclotron limiters and main limiter, and (b) low-hybrid limiters.

The EAST Tokamak is a fully superconducting device with a D-shaped poloidal cross-section and an advanced divertor configuration. Its main parameters include a major radius of $R = 1.85$ m, a minor radius of $r = 0.45$ m, an elongation ratio of $k = 1.2$–2, a maximum plasma current of $I_{\mathrm{P}} = 1$ MA, and a maximum design center toroidal magnetic field of $B_{\mathrm{t}} = 3.5$ T. It is also equipped with a molybdenum first wall and tungsten divertors, and is sufficiently flexible to run in upper or lower single-null and double-null magnetic configurations. Therefore, EAST can be used to study discharges across a variety of parameter ranges. EFIT[34] can be used to obtain the equilibrium configuration of EAST at any given time in cylindrical coordinates, enabling the study of fast-ion loss under various parameters. Similarly, adjusting the NBI and ICRF parameters in TRANSP enabled the calculation of the corresponding fast-ion distribution. Relevant research on this topic is presented in detail in Ref. [12]. Based on this, the fast-ion loss under different heating schemes can be calculated.

This section outlines the necessary conditions and calculation process for determining fast-ion loss. The calculation flowchart is presented in Fig. 3. The distribution of fast ions generated during the NBI+ICRF synergistic process can be calculated through integrated TRANSP simulations, combined with the TORIC and NUBEAM modules and self-consistent iteration of the Fokker–Planck equation (FPP). In this workflow, the FPP solver in the NUBEAM module accounts for collisional effects, fully including fast-ion energy slowing-down, pitch-angle scattering, and associated radial diffusion in the background plasma. Simultaneously, the TORIC module computes the propagation and absorption of ICRF waves and returns the resonant wave acceleration of ions — expressed as an "RF kick" operator — to NUBEAM. By iteratively solving the Fokker–Planck equation, which includes the NBI source, RF kick, and collision terms, a quasi-steady-state fast-ion distribution function is obtained for a given discharge time, self-consistently capturing the balance between NBI injection, ICRF acceleration, and Coulomb collisional slowing-down.[29] This computed quasi-steady-state distribution serves as a realistic initial condition. A large sample of particles is drawn from this distribution and imported into the full-orbit tracking code LORBIT. In LORBIT, these particles are treated as collisionless test particles; their equations of motion include only the Lorentz force, and collisional effects are not included. Using the plasma parameters and magnetic field equilibrium provided by EFIT, the fast ion distribution and magnetic field data were input into the classical guiding orbit program LORBIT to quantitatively analyze fast-ion loss. NUBEAM is a Monte Carlo package developed by Princeton Plasma Physics Laboratory (PPPL) to simulate fast ion deposition, evolution, slowing, and thermalization in tokamaks. It tracks the motion of the fast ions and provides information on their distribution. The full-wave simulation program TORIC employs a finite-Larmor-radius (FLR) approximation to solve the wave equations in the ion cyclotron frequency range for arbitrary axisymmetric geometries, enabling an accurate description of wave propagation and absorption. During the EAST discharge, typical ion motion trajectories can be classified into two categories: trapped and passing ion orbits, corresponding to trapped ion loss and passing ion loss, respectively. Figure 4 shows the actual orbits of the trapped and passing particles in toroidal and poloidal views. In the LORBIT code, the equation for beam ion motion in an electromagnetic field $m\mathrm{d}\boldsymbol{v}/\mathrm{d}t = q(\boldsymbol{v} \times \boldsymbol{B} + \boldsymbol{E})$ is solved using

the sixth-order Runge–Kutta–Gill method, where m, $\boldsymbol{v}$, q, $\boldsymbol{B}$ and $\boldsymbol{E}$ represent the beam ion mass, relative beam ion velocity, beam ion charge, magnetic field, and electric field, respectively. The pitch angle is calculated in the LORBIT code by determining the angle of the velocity vector at the deposition position with respect to the local magnetic field direction, i.e., $\Lambda = \arccos(v_{\parallel}/v)$, where $v_{\parallel}$ is the parallel ion velocity with respect to $\boldsymbol{B}$. The orbital follow time was set to 10^{-3} s, during which the trajectories of 10^5 initial ions were tracked, using a random number generator to select their initial locations. When a particle hit the first wall or limiter, it was considered lost. The initial positions, initial energies, initial pitch angles, final positions, final energies, and final pitch angles of the fast ions were recorded. It is worth noting that the energy and pitch angle of any unlost particles were also recorded after 10^{-3} s. It should be noted that in particle trajectory simulations using the LORBIT code, the continuous wave–particle interactions induced by ICRF are not considered. LORBIT mainly performs trajectory tracking based on the initial particle distribution calculated by TRANSP.

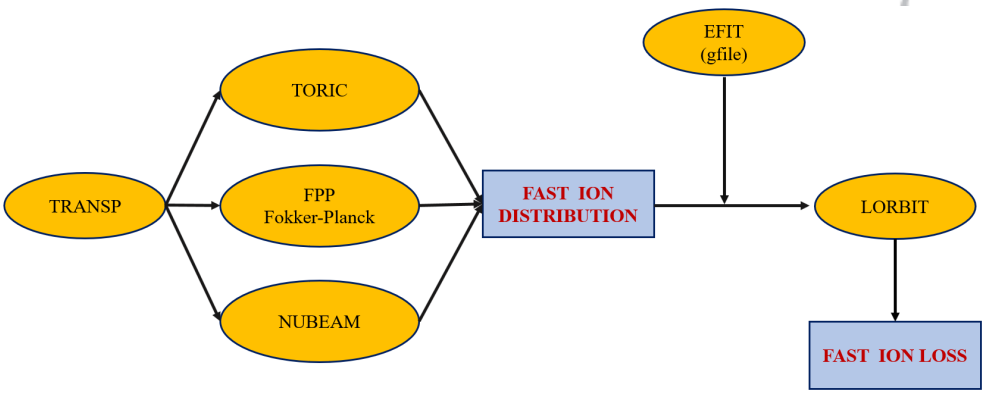


Fig. 3. Flowchart of the predictive analysis of fast-ion loss.

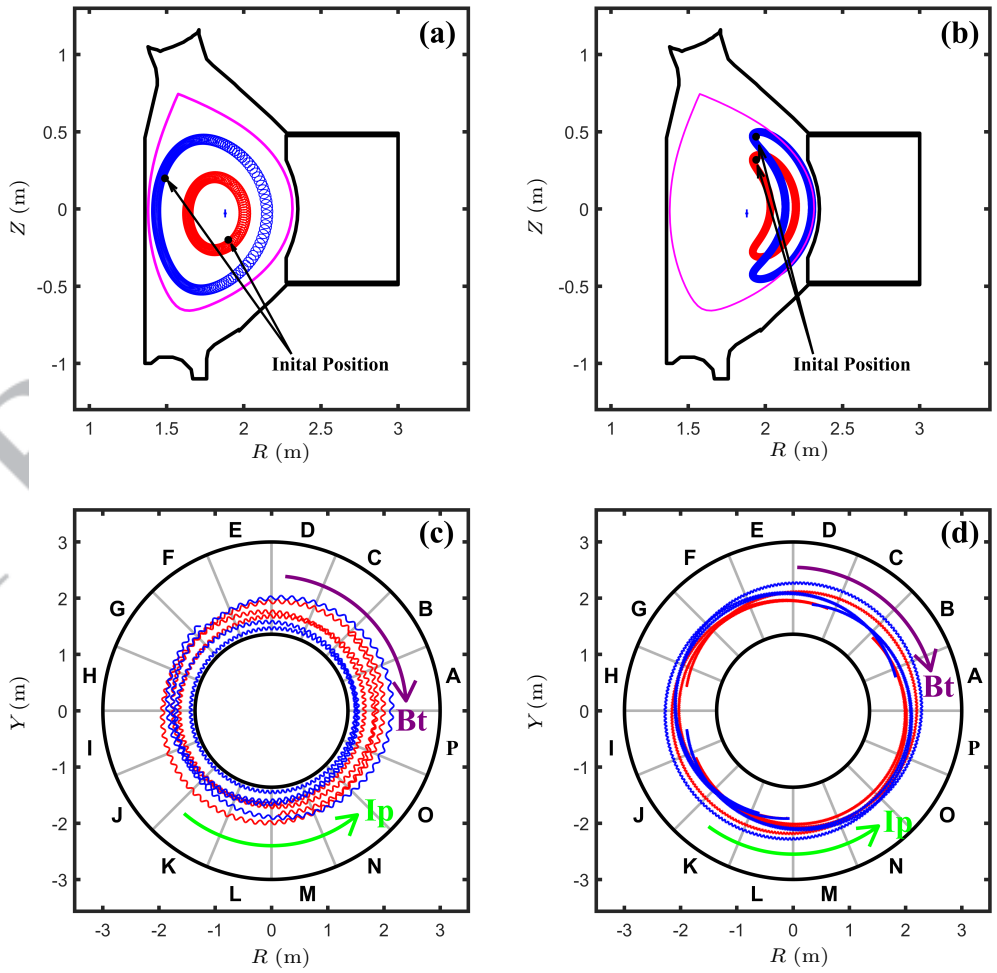


Fig. 4. Examples of the typical trajectories of the fast deuterium ions in the EAST. Passing ions: (a) poloidal view and (c) top view. The initial pitch angles are 55° (red line) and 62° (blue line), respectively. Trapped ions: (b) poroidal view and (d) top view. The initial pitch angles are 89.7° (red line) and 89.3° (blue line), respectively.

3. Result and discussion

In the simulations, the deuterium fast ion distribution generated by TRANSP was used as the input in the LORBIT code to calculate the fast-ion loss. Based on EAST discharge #101735, we calculated the birth distribution of the fast ions generated by NBI1L after heating by ICRF. Figures 5(a) and 5(b) show the spatial birth distributions and pitch energy distributions for NBI1L + ICRF, respectively. ICRF effectively accelerated the NBI ions, leading to the formation of high-energy particle tails, as shown in Fig. 5(b).

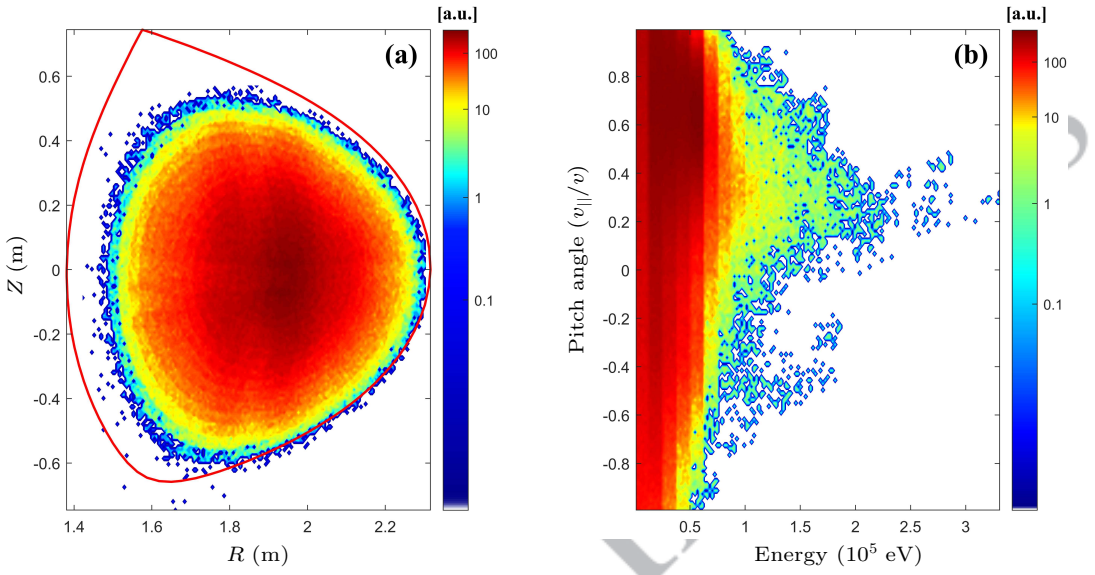


Fig. 5. (a) NBI(1L) fast ion initial spatial distribution (the red line indicates the LCFS). (b) Initial energy–pitch angle distribution.

3.1. Parameter scan of discharge

In this section, various parameters including the plasma current (I_P), toroidal magnetic field (B_t), distance between the antenna and the separatrix (R_{gapout}), position of the strike point (R_X), and divertor configuration are scanned. A reference case used $n(H) = 5\%$, $P_{IC} = 1$ MW, $E_{beam1L} = 55$ keV and an injection angle (with respect to the radial direction) of 15.88°.

Plasma current critically influences key aspects of tokamak operation, including the maintenance of plasma confinement and equilibrium, the provision of ohmic heating, and the evolution of MHD instabilities. Figure 6 shows that the fast-ion loss is primarily distributed in the region below the midplane at $I_P = 300$ kA calculated with LORBIT, owing to the effects of the magnetic field curvature and gradient. Red dots represent the fast ions lost to the first wall or limiters. Further analysis of the fast-ion loss on the limiter (Fig. 7) revealed that the lost ion energy was primarily concentrated in the range of 200–300 keV, and the pitch angle was concentrated at approximately 120°. The value of I_P can have a remarkable influence on fast-ion loss. The results of I_P scans, which record the total loss (T-L), loss at the ion cyclotron antenna limiter (ICA-L), loss at the main limiter (GH-L), loss at the low-hybrid antenna limiter at port B (LHA-L(B)), and loss at the low-hybrid antenna limiter at port E (LHA-L(E)), are shown in Fig. 8. With increasing I_P, the fast-ion loss reduced significantly.

This is primarily because increasing I_P effectively reduces the fast ion orbital width, thereby enhancing plasma confinement. Among all the limiters, the loss of fast ions on the LH limiter at port B was minimal because it was the furthest from the plasma. In addition, it was found that the loss of fast ions was primarily concentrated in the region with a poloidal angle of around −30° in Fig. 9. These results provide valuable guidance for determining the optimal placement of fast-ion loss probes. The magnitude of the toroidal magnetic field, which significantly affects plasma equilibrium and stability, is another key parameter in magnetic confinement fusion devices. Additionally, it governs the magnetic topology, plasma gyroradius, and radial transport, thereby affecting fast ion confinement. Figure 10(a) illustrates the fast-ion loss under different toroidal magnetic field strengths. It is evident that fast-ion loss significantly decreases as the magnetic field strength increases. This is primarily because an enhanced magnetic field reduces the Larmor radius of fast ions, thereby narrowing their drift orbit width and lowering the loss probability.

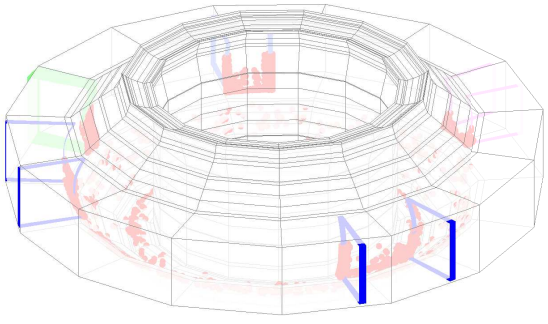


Fig. 6. 3D view of fast-ion loss at $I_P = 300$ kA. The ion cyclotron antenna limiters are shown in blue, the low-hybrid antenna limiters in pink, and the main limiters in green.

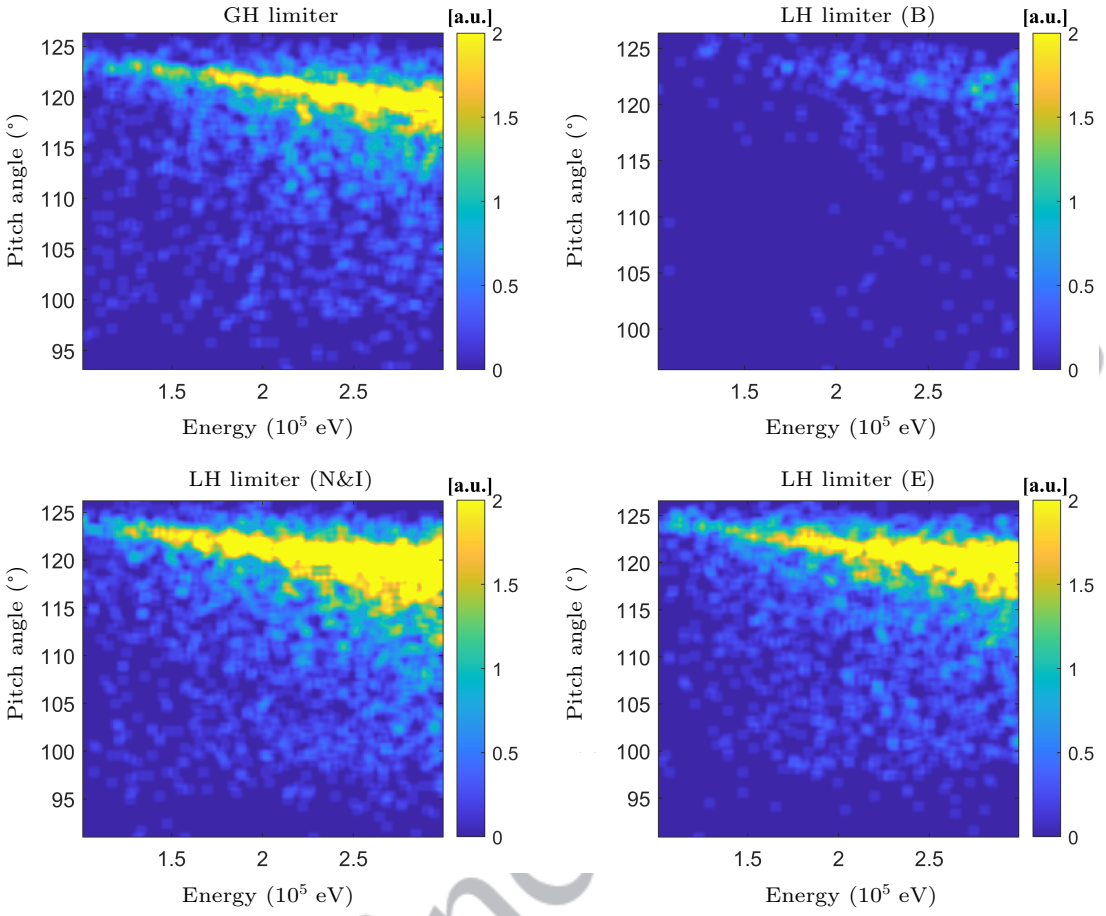


Fig. 7. Distribution of lost fast-ion energy and pitch angle at limiters.

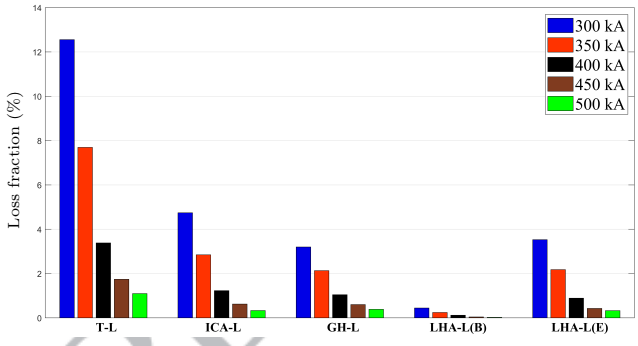


Fig. 8. Comparison of fast-ion loss for cases with different plasma currents.

Subsequently, we considered the influence of the main parameters of the magnetic configuration on the fast-ion loss. The results are shown in Figs. 10(b)–10(d). First, consider the impact of R_{gapout}. As shown in Fig. 10(b), with an increase in R_{gapout}, the proportion of fast ions lost to the first wall and each limiter decreases gradually. In simulations, because the LCFS is not used as the loss boundary, ions that cross the LCFS may still return to it owing to drift motion. Conversely, defining the LCFS as a strict loss boundary would cause an overestimation of the actual particle loss rate. By contrast, increasing R_{gapout} shifts the deposition location of the NBI beam ions toward the plasma core. This leads to a greater proportion of passing particles and a corresponding decrease in the trapped particle ratio, thereby contributing to a reduction in the fast-ion loss. Figure 11 presents the energy–pitch angle distributions of fast ions lost on various limiters at $R_{\text{gapout}} = 4.4$ cm and 8.8 cm. The fast-ion loss becomes negligible when R_{gapout} increases to 8.0 cm.

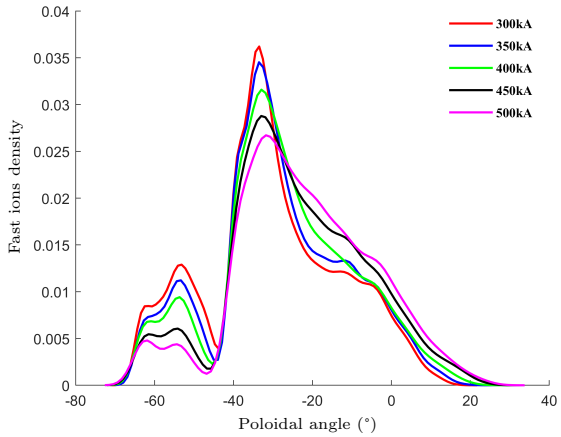


Fig. 9. Poloidal distribution of fast-ion loss.

The divertor configurations also play crucial roles in enhancing the confinement performance of tokamak devices and enabling steady-state, long-pulse operations. Divertors can be categorized into three basic configurations: upper single-null (USN), lower single-null (LSN), and double-null (DN).

In the divertor configuration, the high-energy particles passing through the LCFS are directed along the magnetic field lines to the divertor target plate. The point at which the magnetic field line directly contacts the divertor target plate is known as the strike point. Over the past few decades, extensive research has been conducted on divertors, leading to numerous improvements and optimizations in their geometric configuration, including the development of different configurations such as

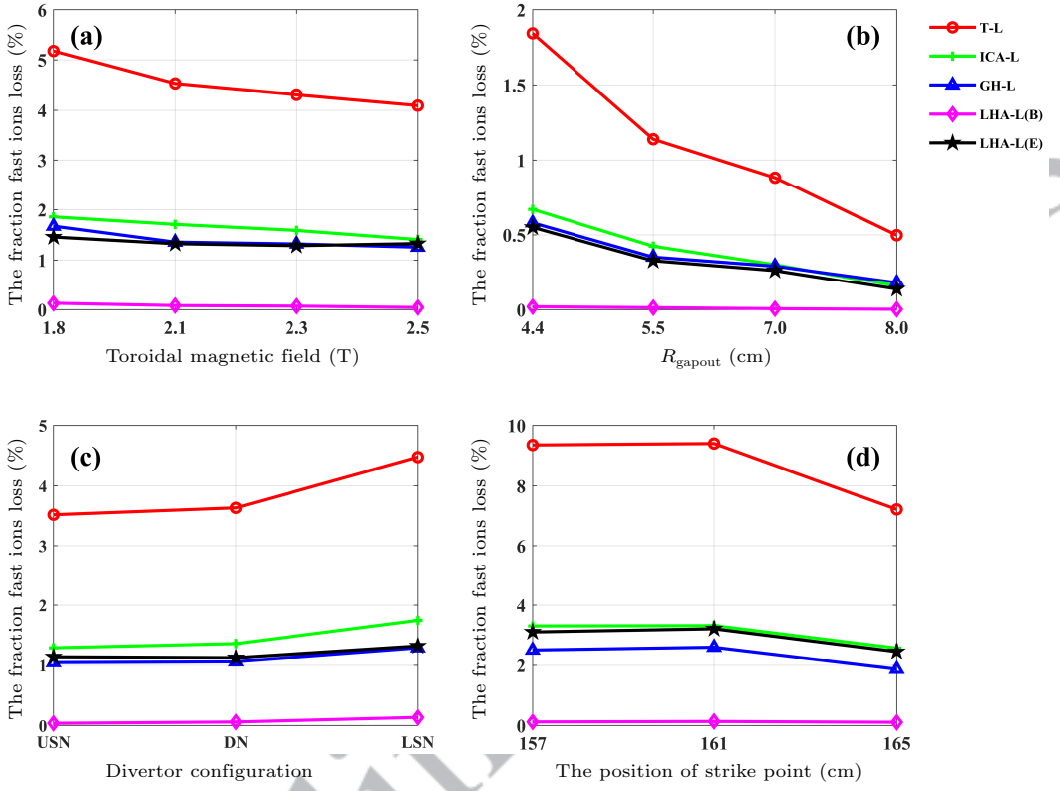


Fig. 10. Comparison of fast-ion loss: (a) toroidal magnetic field (T); (b) R_{gapout}; (c) divertor configuration; and (d) position of Strike point.

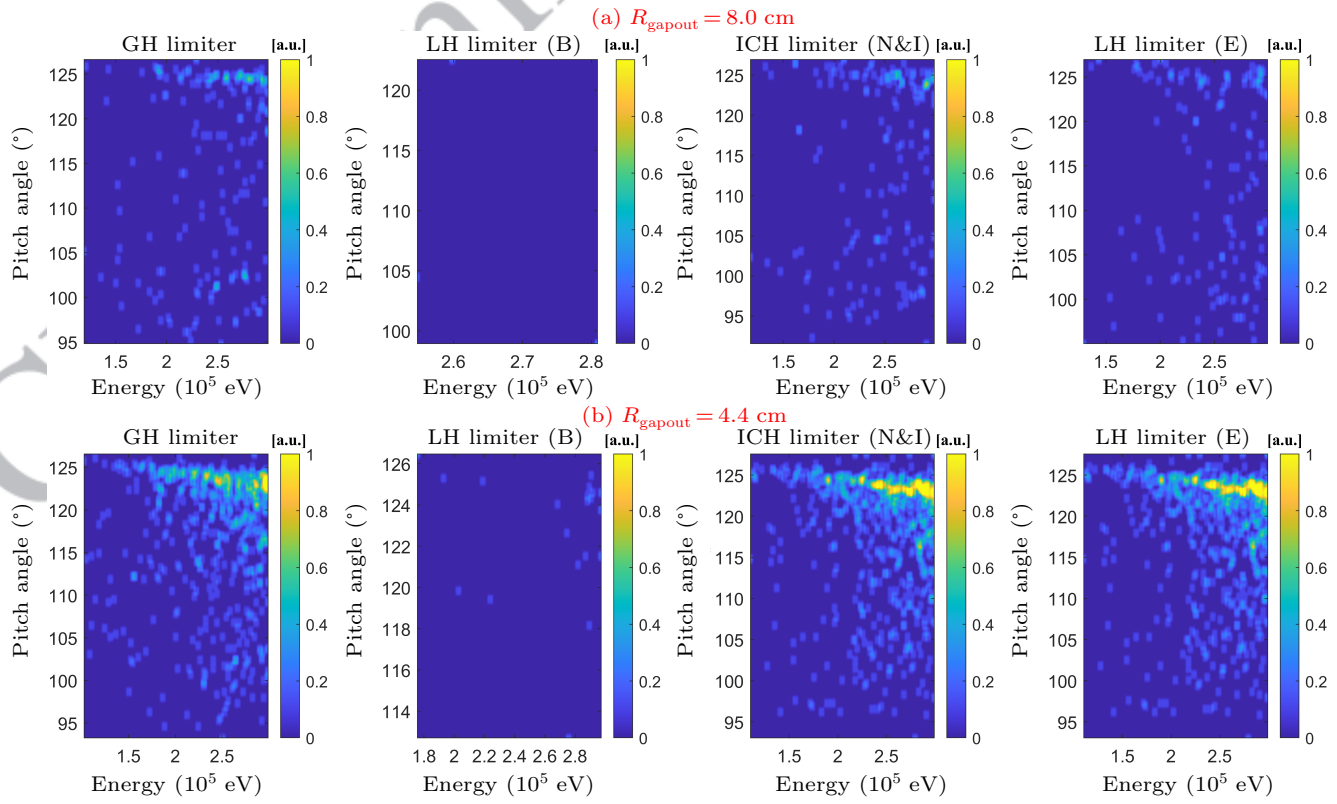


Fig. 11. Energy–pitch angle distributions of fast-ion loss on different limiters, shown for R_{gapout} values of 4.4 cm and 8.0 cm.

parallel and vertical target plates.[35,36] Figure 10(c) presents a comparison of fast-ion loss under different divertor configurations. These results indicate that the LSN configuration results in greater the fast-ion loss, whereas the USN configuration is the most favorable for fast-ion confinement. Therefore, the direction of the toroidal magnetic field must also be considered. In this study, the toroidal field is set to -2.5 T, corresponding to a clockwise orientation when viewed from the top of the EAST. This results in a downward drift direction for charged particles. In this configuration, ∇B and curvature drifts direct ions towards the lower X-point, where the outboard low-field-side region already provides unfavorable curvature for ion confinement. The presence of the lower X-point further enhances this unfavorable curvature and facilitates ion orbit intersection with the lower divertor plates, leading to the strongest loss observed in LSN for $B_t < 0$. This trend is also in line with the well-known concept of unfavorable curvature for ion confinement in tokamaks. Generally, the fast-ion loss are enhanced when their drift direction aligns with the location of the X-point. Conversely, loss are reduced when the drift direction opposes the X-point. Therefore, it is expected that employing a LSN configuration under counter-clockwise B_t would effectively mitigate fast-ion loss. Furthermore, the influence of the strike point position on the divertor target on fast-ion loss was investigated by leveraging the magnetic configuration control capability of the tokamak device. The corresponding results are shown in Fig. 10(d). Flexible control over the strike point location was achieved by adjusting both the radial and poloidal positions of the X-point. Specifically, when the radial position of the X-point (R_X) was removed to 165 cm, the outer strike point was relocated to the vertical target plate, resulting in a significant reduction in the fast-ion loss.

3.2. Parameter scanning of heating

In this section, we change the initial distribution of beam ions in TRANSP by modifying heating modes. Various parameters, including the NBI beam (1L) ion energy and tangential injection radius, were scanned. The effect of the ICRF antenna phase on the fast-ion loss was also considered. The reference case used $n(H) = 5\%$, $I_P = 0.4$ MA, $B_t = -2.5$ T, $R_{gapout} = 4.0$ cm, $R_X = 161$ cm, and double-null divertor configurations. In this study, the magnetic configuration corresponding to discharge #101926 at $t = 5.03$ s was chosen for calculations.

Currently, each beamline in EAST can inject fast ions with energies of up to 80 keV. However, this energy level is insufficient for future fusion devices, such as ITER and CFEDR. Therefore, studying the fast-ion loss induced by NBI injection at different energies is of great significance. In this study, a parameter scan was conducted over injection energies ranging from 40 keV to 80 keV, and the corresponding results are presented in Fig. 12(a). An increase in beam energy results in a significant rise in the number of lost fast ions. Since collisional effects on fast-ion motion were not considered, the observed results align with theoretical expectations. Higher NBI beam energies do not enhance the confinement of fast ions.

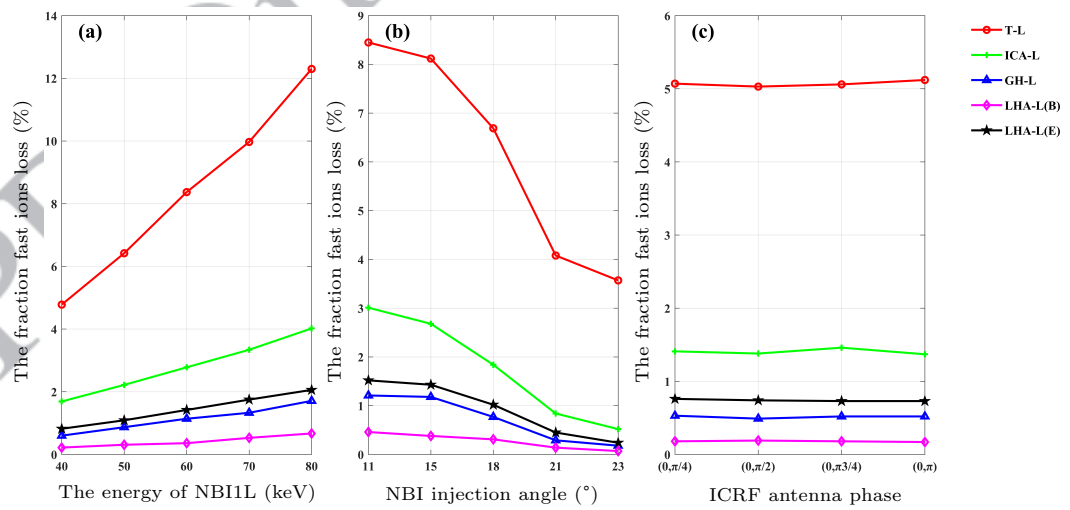


Fig. 12. Comparison of fast-ion loss: (a) energy of NBI; (b) NBI injection angle; and (c) ICRF antenna phase.

The NBI injection angle was then considered. In this study, injection angles (ϕ) of 11°, 15°, 18°, 21°, and 23° were investigated. Notably, for NBI1L, an injection angle of 23° resulted in a more tangential beam trajectory than an injection angle of 11° (Fig. 1). Figure 12(b) compares the fast-ion loss under varying injection angles of NBI1L. The results indicated that the fraction of fast-ion loss decreased as the injection angle increased. The main reason is that the increased injection angle of NBI1L leads to a greater fraction of passing particles, extending the ion trajectory within the magnetic field and consequently improving fast-ion confinement.

Finally, the influence of the ICRF antenna phase on the

CPL Online First Press

fast-ion loss was investigated. The EAST facility is equipped with two types of antennas deployed in separate ports (double-loop and folded-type), with current straps allowing phase adjustments between 0° and 360°. In this study, the impact of four specific phase differences $(0, \pi)$, $(0, \pi/2)$, $(0, 3\pi/4)$, and $(0, \pi/4)$ on fast-ion loss was evaluated numerically. The results presented in Fig. 12(c) indicate that the antenna phase has only a limited effect on the ion loss. This can be explained by the weaker effect of the antenna phase variation on plasma heating relative to the changes in the NBI parameters. While the $(0, \pi)$ phase demonstrates higher heating efficiency, Fig. 5 in Ref. [**?**] indicates only a slight increase in plasma stored energy and core electron temperature under these conditions.

4. Summary

In this study, the loss behavior of fast ions in the EAST during ICRF + NBI synergy under different discharge parameters and heating scenarios was studied using the full orbit following code LORBIT. The initial distribution of the beam ions, accelerated by ICRF waves, was obtained from an integrated simulation using the TRANSP code. In our simulation, the main limiter, radio frequency wave antenna limiter, and first wall were treated as loss boundaries for the first time. Consequently, fast ions are regarded as lost when they strike the first wall or any of the limiters of the EAST, in contrast to the drifting beyond the LCFS. The simulation results indicate that the plasma current (I_{P}), toroidal magnetic field (B_{t}) and R_{gapout} are positively correlated with the proportion of fast-ion loss. The effect of the divertor configuration on fast ion loss is strongly influenced by the direction of the toroidal magnetic field. Fast-ion loss increased when the gradient and curvature drifts of the charged particles were directed toward the X-point, whereas confinement was enhanced when these drifts were oriented away from it. Additionally, selecting a double-null magnetic configuration and positioning the strike point on the vertical target plate can enhance the confinement of fast ions. Finally, the effects of the NBI injection angle, injection energy, and ICRF antenna phase on fast-ion loss were numerically investigated. The results indicated that, in the absence of collisions and within a certain range, the fast-ion loss fraction gradually decreases with increasing NBI injection angle. Conversely, increasing the injection energy exacerbates fast ion loss. Moreover, the ICRF antenna phase has only a marginal influence on both the fast-ion loss and confinement.

Furthermore, the LORBIT code employed in this study is capable of simulating ion, electron, and impurity orbits, making it suitable for investigating impurity emissions, ion transport, and associated processes. However, the current model only treats fast ions generated by the ICRF-NBI synergy as an input source, without considering the continuous influence of the ICRF wave field during fast-ion propagation and loss. The code can only track the collisionless orbit after obtaining the particle distribution function and performing self-consistent processing. This integrated simulation of the process has not yet been realized; therefore, it will be the focus of future research.

Acknowledgments

Project supported by National Magnetic Confinement Fusion Energy Development Research Project of China (Grant Nos. 2022YFE03190200 and 2019YFE03070000), the National Natural Science Foundation of China (Grant No. 12175273), the Comprehensive Research Facility for Fusion Technology Program of China (Grant No. 2018-000052-73-01001228), and the Strategic Priority Research Program of Chinese Academy of Sciences (Grant No. XDB0790203).

References

[1] Hu C, Xie Y, Xie Y, Liu S, Xu Y, Liang L, Jiang C, Sheng P, Gu Y, Li J and Liu Z 2015 *Plasma Sci. Technol.* **17** 817
[2] Wang J F, Wu B and Hu C D 2010 *Plasma Sci. Technol.* **12** 289
[3] Zhang W, Zhu G H, Zhang X J, *et al.* 2023 *Nucl. Fusion* **63** 056015
[4] Cordey J G 1976 *Nucl. Fusion* **16** 499
[5] Garcia-Munoz M, Fahrbach H U, Guenter S, Igochine V, Mantsinen M J, Maraschek M, Martin P, Piovesan P, Sassenberg K and Zohm H 2008 *Phys. Rev. Lett.* **100** 055005
[6] Ogawa K, Isobe M, Toi K, Shimizu A, Spong D, Osakabe M, Yamamoto S and the LHD Experiment Group 2013 *Nucl. Fusion* **53** 053012
[7] Tani K, Azumi M, Kishimoto H and Tamura S 1981 *J. Phys. Soc. Jpn.* **50** 1726
[8] Zhang W, Hu L Q, Sun Y W, Ding S Y, Zhang Z J and Liu S L 2014 *Chin. Phys. B* **23** 105201
[9] Bolte N, Heidbrink W W, Pace D C, Van Zeeland M A and Chen X 2015 *APS Meeting*
[10] Porcelli F, Eriksson L G and Furno I 1996 *Phys. Lett. A* **216** 289
[11] Forest C B, Ferron J R, Gianakon T, Harvey R W, Heidbrink W W, Hyatt A W, La Haye R J, Murakami M, Politzer P A and St. John H E 1997 *Phys. Rev. Lett.* **79** 427
[12] Duong H, Heidbrink W, Strait E, Petrie T, Lee R, Moyer R and Watkins J 1993 *Nucl. Fusion* **33** 749
[13] Li J and Wan Y 2021 *Engineering* **7** 1523
[14] Hu C D 2021 *Plasma Sci. Technol.* **14** 567
[15] Chang J F, Isobe M, Ogawa K, Huang J, Wu C R, Xu Z, Jin Z, Lin S Y and Hu L Q 2016 *Rev. Sci. Instrum.* **87** 427
[16] Isobe M, Funaki D and Sasao M 2009 *J. Plasma Fusion Res. SERIES* 8
[17] Wang F, *et al.* 2021 *Chin. Phys. Lett.* **38** 055201
[18] Xu Y, Guo W, Ye L, Xiao X, Wang S and Zhu S 2018 *Phys. Plasmas* **25** 012502
[19] Wang F, Wan J B, Lin Z H, Wu X F and Wang Z X 2025 *Application of Particle Orbit Tracking Model in Tokamak Burning Plasmas* presented at the 9th Asia-Pacific Conference on Plasma Physics, Fukuoka, Japan, Sep. 21–26
[20] Zheng Y, Xiao J, Hao B, Xu L, Wang Y, Zheng J and Zhuang G 2022 *Chin. Phys. B* **31** 075201
[21] Sipilä S, Varje J, Johnson T, Bilato R, Galdón-Quiroga J, Snicker A, Kurki-Suonio T, Sanchís L, Silvagni D, González-Martín J, the ASDEX Upgrade Team and the EUROfusion MST1 Team 2021 *Nucl. Fusion* **61** 086026
[22] Kramer G J, *et al.* 2013 *Plasma Phys. Control. Fusion* **55** 025013
[23] Pfefferlé D, Cooper W A, Fasoli A and Graves J 2016 *Nucl. Fusion* **56** 112002
[24] Xu Y, *et al.* 2020 *Nucl. Fusion* **60** 086013
[25] Song C, Wang J, Wu B, Yin L, Gong X, Hao B, Chen Y, Huang Q, Zhong Y, Xie Y and Xie Y 2024 *Plasma Phys. Control. Fusion* **66** 075003

CPB Online First Press

[26] Song C, Wu B, Gong X, Wang J, Chen Y, Hao B, Ti A, Wang S, He L, Zhong G, Yin L, Li J, Cui Z, Huang Q, Zhong Y, Xie Y and Xie Y 2022 *Plasma Phys. Control. Fusion* **65** 025003
[27] Xu Y, Li L, Hu Y, Liu Y, Guo W, Ye L and Xiao X 2020 *Nucl. Fusion* **60** 086013
[28] Hawryluk R J 1981 *Physics of Plasmas Close to Thermonuclear Conditions* 19
[29] Breslau J, Gorelenkova M, Poli F, Sachdev J, Pankin A, Perumpilly G, Yuan X and Glant L 2018 *Computer Software*
[30] Pankin A, McCune D, Andre R, Bateman G and Kritz A 2004 *Comput. Phys. Commun.* **159** 157
[31] Pankin A, Bateman G, Budny R, Kritz A, McCune D, Polevoi A and Voitsekhovitch I 2004 *Comput. Phys. Commun.* **164** 421
[32] Bilato R, Brambilla M, Horton L, Maggi C and Stober J 2009 *Radio Frequency Power in Plasmas: Proceedings of the 18th Topical Conference* **1187** 81
[33] Brambilla M 2002 *Plasma Phys. Control. Fusion* **44** 2423
[34] Qian J P, Wan B N, Lao L L, Shen B, Sabbagh S A, Sun Y W, Liu D M, Xiao B J, Ren Q L, Gong X Z and Li J G 2009 *Plasma Sci. Technol.* **11** 142
[35] Zhu S Z and Zha X J 2005 *Plasma Sci. Technol.* **7** 2897
[36] Zhou Z, Yao D and Cao L 2015 *J. Fusion Energy* **34** 93

CPB Online In-Press